Iranian Journal of Catalysis 9(3), 2019, 201-211

IRANIAN JOURNAL OF CATALYSIS

Preparation of ZnO nanocatalyst supported on todorokite and photocatalytic efficiency in the reduction of chromium (VI) pollutant from aqueous solution

Maryam Sabonian, Kazem Mahanpoor*

Department of Chemistry, Arak Branch, Islamic Azad University, Arak, Iran.

Received 16 October 2018; received in revised form 03 February 2019; accepted 20 March 2019

ABSTRACT

In this research, a new effective photocatalyst was prepared by supporting ZnO on a Todorokite (TD). This catalyst was characterized by employing the scanning electron microscopy (SEM-EDX) and X-Ray Diffraction (XRD) patterns. The optical properties of the samples were measured by the diffuse reflectance spectroscopy (DRS). The purpose of using the ZnO/TD as a photocatalyst was to reduce Cr(VI), which is a pollutant in water. Experiments were carried out under different operating conditions including an initial concentration of Cr(VI), photocatalyst amounts and pH values. To optimize processes and obtain a mathematical model, the researcher used a full factorial design (with three factors at three levels). The optimal conditions were determined where the amount of photocatalyst= 200 mg L^{-1}, pH= 2 and the concentration of Cr(VI)= 15 ppm. The reduction efficiency in an optimal condition was 97.73%. The experimental results showed that kinetic was the first order and k= 0.1489 min^{-1}.

***Keywords**: Todorokite, Photocatalytic reduction, Cr(VI), ZnO nanoparticles, Full factorial experimental design.*

1. Introduction

Recent research efforts have concentrated on photocatalytic reduction of Cr^{6+}, which is a pollutant in aqueous solution. Cr(VI) is a toxic pollutant found in different industrial wastewaters including leather tanning industries, chrome plating, metallurgical, electronic and so on [1]. Cr^{6+} and Cr^{3+} are two usual oxidation states of chromium, but Cr(VI) is relatively much more toxic and carcinogenic. Indeed, Cr^{3+} in low doses is an essential dietary mineral [2]. The concentration of Cr^{6+} in industrial sewage ranges from 0.5 and 270 mg L^{-1} [1]. The hexavalent state may be found in the form of chromic acid (H_2CrO_4), dichromate anion ($Cr_2O_7^{2-}$), hydrogen chromate anion ($HCrO_4^-$) or chromate anion (CrO_4^{2-}) [1]. The Cr^{6+} form is five hundred times more poisonous than the Cr^{3+} form [2]. Moreover, it has toxic and damaging effects on various organs of the human body [3]. Common methods of Cr(VI) removal includes chemical materials, ion replacement, adsorption of coal or active carbon and bacterial reduction [4].

*Corresponding author.
E-mail address: k-mahanpoor@iau-arak.ac.ir (K. Mahanpoor)

However, these methods have disadvantages; most of the existing methods are expensive or require many chemicals. Some also produce a secondary sewage. In addition, some of these methods require advanced techniques and instruments.

Advanced oxidation process (AOPs) is one of the most important methods for the removal of water pollutants. This method was done in company with different methods. A photocatalytic procedure is one of the most important and practical AOPs methods. The photocatalytic methods are based on the properties of electron-hole pairs produced in the semiconductor after having been illuminated by a light which has more energy than the semiconductor band gap [5]. The organic compounds such as dyes were oxidized by the generated hydroxyl and peroxide radicals through the photocatalytic process [6]**.** These processes are called photocatalytic oxidation. In addition, based on the mechanism of an electron-hole, and due to the presence of electrons in the conduction band and also the cavity in the valence band, there is a possibility of reduction reactions to absorb the metal ions such as chromium. These processes are called photocatalytic reduction.

A photocatalytic reduction can be based on electron absorption of metal ions from the conduction band directly or from reactions to the hole indirectly. For chromium (VI) ions, there is a possibility of the photocatalytic reduction reaction in both ways [7,8].

The various forms of chromate in aqueous solutions species are in a chemical equilibrium. The most important factor of the prevailing species in the solution is pH. In solutions that are alkaline or weakly acidic, the dominant species are chromate (CrO_4^{2-}) or hydrogen chromate anion ($HCrO_4^-$). In strong acidic solutions, the dominant species is dichromate ($Cr_2O_7^{2-}$) [9]. The Photocatalytic reduction of Cr^{6+} is possible with semiconductors like ZnO, TiO2, ZnS, CdS and WO3 [10].

Transition metals are popular since they are active species in many artificial catalytical processes. The transition-metal based octahedral molecular sieve (OMS) promises simpler and more effective incorporation of various active transition-metal species. A porous manganese oxide with an octahedral coordinated structure has attracted much notice due to its controllable structures, porosities, and catalytical selectivity compared to those of tetrahedral porous materials. These superior benefits have raised many useful applications of manganese oxide OMS in the catalysis, semiconductors, ion-exchange, radioactive hazard separation, sensors, and batteries. A Todorokite is one kind of manganese oxide. It is mined as an ore of manganese and made up of ($Mn^{4+}O_6$) octahedral that shares edges to form triple chains. The unit cell has six manganese Mn^{4+} sites and twelve oxygen O^{2-} sites constituting the octahedral framework. These chains use corners to create square tunnels. The crystalline manganese oxides have the largest tunnels; therefore, they are able to absorb inorganic harmful ions such as heavy metals or small molecules inside the tunnel. The properties of these compounds are similar to zeolites. Due to their unique properties such as mechanical and thermal strength and high porosity, these compounds can be used as the base of a zinc oxide photocatalyst.

The ZnO is widely employed in catalysts, sensors, piezoelectric, optoelectronics, semiconductors for solar cells and water treatment processes, and transducers in medical sciences [11-13]. The zinc oxide optical band gap is 3.37 eV. Thereby, it is a semiconductor with a high photocatalytic property. Other properties of the zinc oxide such as insolubility in water, high chemical stability, non-toxic and low cost are suitable for the photocatalytic reduction process [14,15].

Zinc oxide particles are very small; thus, it is difficult to separate them from water after using it as a photocatalyst. One of the ways to solve this problem is to fix these particles on a suitable base. In this way, the size of the catalyst particles will be larger and the separation will be easier. In addition, the catalytic activity usually increases due to the catalyst stabilization on the base.

Studies have shown that a Todorokite exhibits dehydration and cation-exchange behavior similar to many zeolites suggesting a possible potential for a base of a catalyst [16].

The purpose behind the application of different techniques is to design experiments, classify the factors affecting the process and determine the optimal values. With the help of DOE techniques, researchers can, at first, determine the variables that have the greatest influence on the output. Second, the effective input variables are determined to match the response values to their nominal values, to minimize their variability and to respond to the uncontrollable factors of the variable. The most important techniques for designing experiments are statistical techniques such as analysis of variance (ANOVA), factorial designs, regression methods, so on.

To optimize the photocatalytic reduction process, it is essential that the researcher examine all the variables that affect the process. It is difficult to examine the individual effects of the process, especially if these factors influence each other. The interactions of various agents can only be examined by a design of experiments (DOEs) which can eliminate these problems. The design of experiments is a strong method used to detect a collection of process factors (or variables) which are the most significant to the process; then, to define at what levels these factors must be held so that the process efficiency is optimized. A statistical design of experiments is a fast and affordable method to understand and optimize any construction processes.

A full factorial experimental design can decrease the number of tests and optimize all the effective factors that have effects on the results of experiments. It is a proper method of DOEs [17].

A full factorial methodology is a set of statistical techniques and applied mathematics to model experimental results. This method can check the efficiency of various factors (with various levels) and their effects on each other [18-20].

If all variables are measurable, a full factorial experimental design can function as follows:

$$Y = f(x_1, x_2, x_3 \dots x_i) \quad (1)$$

The target is the optimization of response Y. The assumption is that the variables (x_1, x_2) are independent and the error is negligible. Then, an appropriate

approximation for the functional relationship between the independent variables and the first order equation can be assuredly determined. A factorial designs conclusion 11 tests all possible mixtures of x_1, x_2 and x_3. The photocatalytic reduction efficiency (Y) was measured for every test. The researcher selected the first-order equation to fit the experimental data (with all possible effects):

$$y = \beta_\circ + \sum_{i=1}^{k} \beta_i x_i + \sum_{1\le i\le j}^{k} \beta_{ij} x_i x_j \qquad (2)$$

Where k is the number of variables, β_0 is a constant, β_i represents the coefficients of the linear parameters, the constant β_{ij} represents the coefficients of the interaction parameters, x_i and x_j are the variables [21].

The purpose of this study is to use a Todorokite as a new base for the stabilization of the ZnO photocatalyst and identification for the first time. The ZnO/TD photocatalytic activity has been investigated to remove the Cr(VI) aqueous solution. The researcher employed an experimental design method to optimize and present an appropriate mathematical model. In this research, a three-factor and three-level full factorial experimental design was used for photocatalytic reduction of Cr^{6+} process.

2. Experimental

2.1. Materials

Potassium dichromate, sulfuric acid and sodium hydroxide $MnCl_2$ $4H_2O$, $MgSO_4$ $7H_2O$, $K_2S_2O_8$, urea and zinc nitrate were purchased from the Merck company (Germany).

2.2. Catalyst production procedure

The researcher used a hydrothermal method based on previous studies to prepare a Todorokite [22]. A 6.0 M NaOH solution (30 ml) was added drop by drop to an $MnCl_2$ solution (which was prepared by the dissolution of 1.98 g of $MnCl_2$ $4H_2O$ in 15 ml of distilled water) for 15 min. Then, 1.89 g of $K_2S_2O_8$ and 0.344 g of $MgSO_4$ $7H_2O$ were added for 30 min to form the yellow precipitate of manganese hydroxide (II). The precipitate was mixed with 200 ml of 1.0 M $MgSO_4$ solution for 12 h. The product was subjected to a hydrothermal treatment by a hermetic Teflon cell filled with distilled water 75–85% by volume. An autoclave with its cell was put in an oven (160 ℃) for 24 hours. The autoclave was taken from the oven and cooled down for 8–12 h so that it reached the room temperature. The crystalline deposit (Mg Todorokite) was washed in distilled water for several times until there is no reaction to Cl^-. The researcher obtained the H-Todorokite by holding the Mg-Todorokite in the 1.0 M HNO_3 solution for 48 h under mixing of a suspension with a magnetic mixer. The H-Todorokite precipitates were repeatedly washed in distilled water until pH= 7.

2 g of the Todorokite powders was added to 25 ml of 5.0 M Zinc nitrate and, then, was shacked for 2 hours. Thereafter, 25 ml of 2.0 M urea solution with a temperature of 90-95 ℃ was added to the mixture and put in a water bath for 6 hours. The sediments were separated by a filter paper, dried at an ambient temperature, and placed in a furnace at 350 ℃ for 3 hours. The researcher characterized this catalyst using a scanning electron microscopy (SEM-EDX) and obtained the Philips Model XL-30 and X-Ray Diffraction (XRD) patterns using DX27-mini. In addition, to determine the optical property of catalyst, the researcher employed the Diffuse Reflection Spectroscopy (DRS) (model DRA-CA-30I).

2.3. Full factorial experimental design

This study investigated the photocatalytic effect of the pure ZnO/TD on the Cr(VI) reduction using DoE. The experiments design considered three variables including pH, the primary concentration of Cr(VI), and catalyst dosages at three-levels and three central points. The values of the selected levels were chosen according to the previous research [23-28]. The pH changed from 2 to 4 at three levels (2, 3 and 4), the primary concentration of Cr(VI) changed from 15 to 25 ppm at three levels (15, 20 and 25 ppm) and the catalyst dosage from 100 to 200 mg L^{-1} at three levels (100, 150 and 200 mg L^{-1}). The removal efficiency of the Cr(VI) was a dependent response. In order to perform the DOEs and analyze the results, the researcher utilized the Minitab 17 version 2.1 statistical software and an analysis of variance (ANOVA), respectively.

2.4. General procedure

A photocatalytic reactor was used in this work. An MDF box was designed in which a batch Pyrex reactor with 500 ml capacities was placed. On the upper section of the box, three mercury lamps (Philips 15W) were built-in as the UV light sources. The radiation is produced almost individually at 254 nm. These lamps were set at in a 10-cm distance so that the light was evenly emitted on the box due to the liquid inside the reactor. The contents of the reactor were mixed by a magnetic stirrer and the air intranet the box was ventilated by a fan (behind the box). For each experiment, first, 250 ml Cr(VI) solution was made as a specified concentration and poured inside the reactor. At a certain

pH, the defined amount of catalyst was added to the reactor. In all experiments, pH adjustment was done via the minimum use of H_2SO_4 and NaOH. To initiate the process, the researcher instantly turned the stirrer and the UV lamps on. Sampling was done by a 5-ml syringe every 10 min. In order to fully separate the catalyst from solution, the researcher centrifuged the samples for 3 min with a 3500-rpm speed. The Cr(VI) concentration of the samples was determined using an UV/Vis spectrophotometer (Agilent-8453) at λ_{max}= 350 nm. The percentage of the primary concentration of the Cr(VI) was reduced by the photocatalytic process (the percent of photoreduction efficiency); a function of time is given by equation 3:

$$\text{Cr reduction\% (R\%)} = [(A_0 - A_t)/A_0] \times 100 \qquad (3)$$

In this equation A_0 and A_t are the Absorption of Cr(VI) solution at λ_{max}= 350 in time= 0 and times= t, respectively.

3. Results and Discussion

3.1. Characterization of the ZnO/Todorokite

3.1.1. XRD pattern

An XRD is one of the most important characterization tools used in solid state chemistry and materials science. Fig. 1 illustrates an XRD pattern of the ZnO, Todorokite and ZnO/Todorokite. This pattern indicates that the characteristic peaks corresponded to the Todorokite appeared well according to the standard data for Todorokite (JCPDS-38-475) [29] and ZnO (JCPDS-88-0287) [30,31]. It means that the synthesized Todorokite crystals were well formed, and the supporting of ZnO has no appreciable effect on the crystal phase of ZnO and Todorokite. In the pattern, the characteristic peaks of the Todorokite appeared well indicating that the ZnO was stable during the supporting process. Also, the characteristic peaks of the ZnO appeared and these peaks agreed with the results of researchers [22]. The crystalline size is determined by the Debye- Scherrer equation [30]:

$$D = k\lambda/\beta\cos\theta \qquad (4)$$

Where D is the crystalline size, k is constant (it equals to 0.89), λ is the wavelength of the X-rays source, β is the full width half maximum (FWHM) of the 2θ peak and θ is the angle of the X-rays pattern. The average crystalline size of ZnO, NPs before supporting on TD associated with all the diffraction peaks was estimated to be about 37.52 nm and for ZnO NPs after supporting on the TD was calculated 37.83 nm. The results revealed that there was not a significant change in the crystalline size of the ZnO after supporting on the TD.

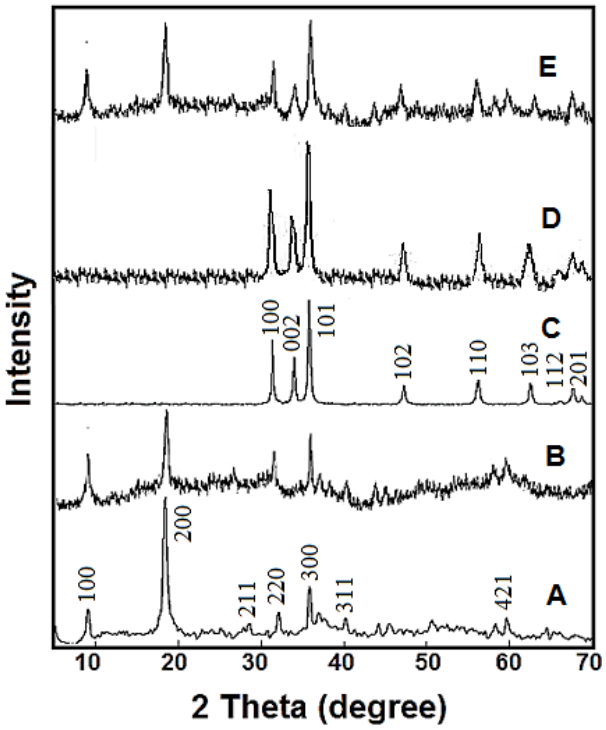

Fig. 1. X-ray diffractogram of the Todorokite [22] (A), synthesized Todorokite (B), ZnO [32] (C), ZnO synthesized (D) and synthesized ZnO/Todorokite (E).

3.1.2. SEM-EDX

The SEM illustration of the synthesized Todorokite is shown in Fig. 2. The surface morphology of the Todorokite shows that this product has suitable structural properties to be used as the base of the catalyst. In other words, the pores existing on the surface of the Todorokite (as a support) supply a suitable condition to support ZnO nanoparticles (NPs). Fig. 2 shows the SEM/EDX of the ZnO/Todorokite. In the RDX spectrum, the peaks of two main elements in the ZnO/Todorokite namely Mn and Zn appeared and were named. Mn is related to the Todorokite catalyst support and Zn is related to the ZnO NPs.

3.1.3. Optical property by DRS

The optical properties of the TD, ZnO and ZnO/TD samples were measured by the diffuse reflectance spectroscopy (DRS) (Varian Cary 100 UV-Vis Spectrophotometer with DRA-CA-30IDiffuse Reflectance Accessory). The band gap energy can be roughly calculated by the $E_g = 1240/\lambda_{onset}$ formula, where λ_{onset} is the absorption onset wavelength. As a consequence, the TD, ZnO and ZnO/TD band gap energy is estimated to be 3.31, 3.18 and 2.96 eV, respectively (Fig. 3). The ZnO/TD band gap energy is lower than TD and ZnO, so it is a more efficient photocatalyst.

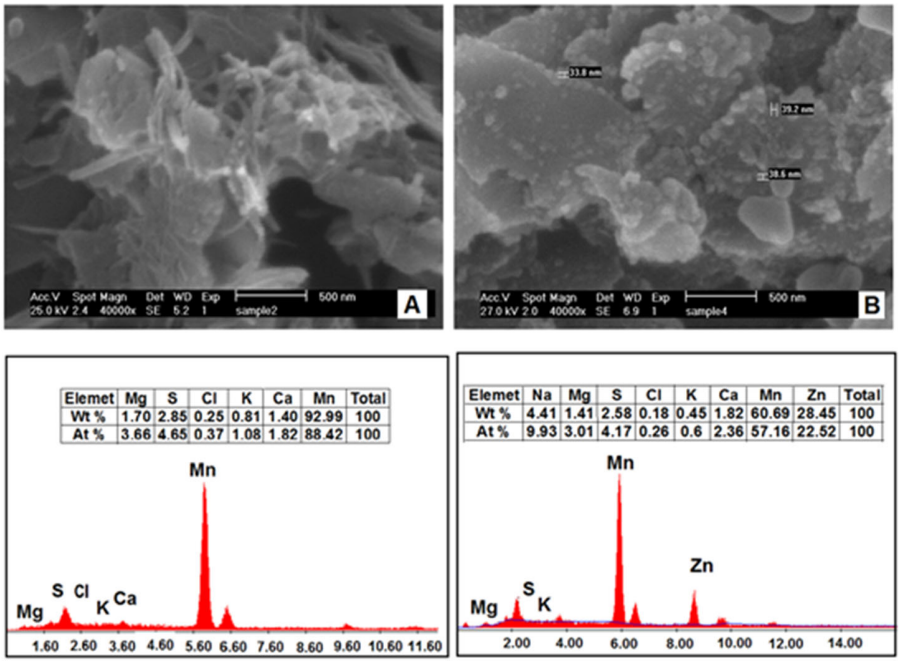

Fig. 2. SEM-EDX result of ZnO/Todorokite prepared by SSD method.

3.2. Photocatalytic mechanism

Fig. 4 shows the schematic presentation of the mechanism of the photocatalytic reduction process of Cr(VI). Under UV irradiation, electron–hole pairs were generated in the surface of the ZnO/TD NPs. The electrons (in conduction bond) reduced the Cr(VI) to Cr(III) and the holes (in valence band) might finally lead to generation of H_2O_2 [32].

Under UV irradiation, electron–hole pairs were generated at the surface of ZnO/TD NPs. After the dissociation of the electron–hole pairs, the electrons reduced Cr(VI) to Cr(III), and the holes might lead to the generation of O_2 in the absence of organics [33].

$$ZnO/TD \xrightarrow{h\upsilon} ZnO/TD\ (e^-/h^+) \quad (5)$$

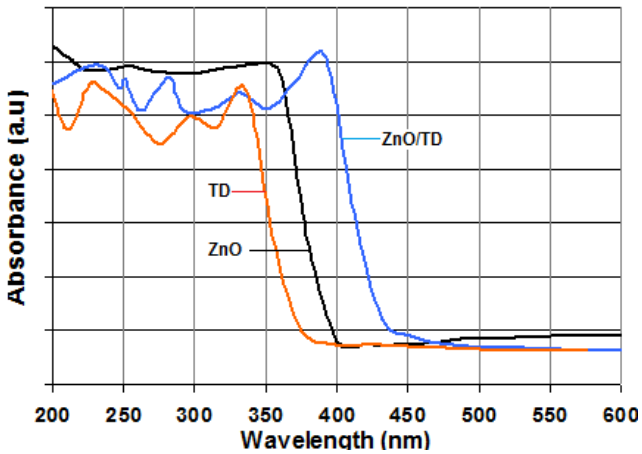

Fig. 3. UV–vis diffuse reflectance spectra of TD, ZnO and ZnO/TD.

In the aqueous solution with different pHs, chromate exists in following ionic forms [9]:

$$Cr_2O_7^{2-}\ (pH < 4) \leftrightarrow HCrO_4^-(pH\ 4-6) \leftrightarrow CrO_4^{2-}\ (pH > 6.5) \quad (6)$$

These ions can react with electrons in the conducting band as follows:

$$Cr_2O_7^{2-} + 14H^+ + 6e^- \rightarrow 2Cr^{3+} + 7H_2O\ E^0 = +1.33\ V \quad (7)$$

$$HCrO_4^- + 7H^+ + 3e \leftrightarrow Cr^{3+} + 4H_2O\ E^0 = +1.48\ V \quad (8)$$

$$CrO_4^{2-} + 8H^+ + 3e^- \rightarrow Cr^{3+} + 4H_2O\ E^0 = +1.33\ V \quad (9)$$

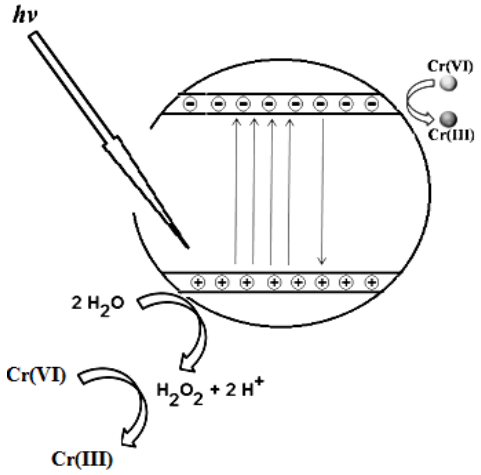

Fig. 4. Schematic representation of the photoreduction process of Cr(VI).

Water can react with a hole as follows and electrons are placed in the hole in the valence band:

$$2H_2O \rightarrow H_2O_2 + 2H^+ + 2e^- \; E^0 = -1.776\,V \quad (\mathbf{10})$$

In addition, H_2O_2 can react with Cr(VI) as follows:

$$Cr_2O_7^{2-} + 3H_2O_2 + 8H^+ \rightarrow 2Cr^{3+} + 7H_2O + 3O_2 \quad (\mathbf{11})$$

However, for the full reduction of the Cr(VI) in the solution, more concentrated solutions and more irradiation time are necessary. This may be due to the fact that increasing the concentration of Cr(VI) hinders the light to completely penetrate into the solution.

As shown in Fig. 5, as the amount of the ZnO/TD photocatalytic increases, the reduction reaction of Cr(VI) increases as well because it enhances the speed of electron formation in the conduction band that is formed under UV radiation.

The detection of various chromium ions in aqueous solutions is very important in photocatalytic processes. Chromium ions are in equilibrium in the aqueous solution**.** Acidity is the most important parameter in these equilibria. The sub-species reactions to equilibrium are shown below:

$$H_2CrO_4 \leftrightarrow H^+ + HCrO_4^- \; (K_1: 1.21) \quad (\mathbf{12})$$

$$HCrO_4^- \leftrightarrow H^+ + CrO_4^{2-} \; (K_2: 3 \times 10^{-7}) \quad (\mathbf{13})$$

$$2HCrO_4^- \leftrightarrow Cr_2O_7^{2-} + H_2O \; (K_3: 35.5) \quad (\mathbf{14})$$

$$HCr_2O_7^- \leftrightarrow H^+ + Cr_2O_7^{2-} \; (K_4: 0.85) \quad (\mathbf{15})$$

It is shown that, when pH < 6.5, only $HCrO_4^-$ and $Cr_2O_7^{2-}$ anions mostly exist and their concentrations become independent of the pH in the 2-5 pH range**.** In a pH > 6.5 condition, the Cr(VI) is mainly present as the CrO_4^{2-} anion. It is significant to note that the chromate compounds are strong oxidizing agents; thus, Cr(VI) has a trend to be reduced to Cr(III). The potential for the dichromate reduction in a strong acidic solution (E^0 = +1.33 V) of the reaction equation (6) confirms that this ion can easily receive electrons. Therefore, it takes the electrons from the conduction band and converts to Cr(III) ions. Dichromate ions ($Cr_2O_7^{2-}$) turn to chromate (CrO_4^{2-}) ions in poorly acidic solutions and also neutral solutions (pH > 6.5). The reduction potential for converting CrO_4^{2-} to Cr^{3+} (reaction (8)) is negative (E^0 = +1.48 V). Therefore, they tend to receive electrons. Based on the reaction (10), the water molecules can lose their electrons and convert them into hydrogen peroxide molecules. The potential for this reaction is negative (E^0 = -1.776 V). These electrons are placed in the hole in the valence band and the hydrogen peroxide is formed. H_2O_2 reacts with dichromate ions in the acidic solution and the Cr(III) ions are produced (reaction 11).

In acidic solutions, the dominant species is dichromate ($Cr_2O_7^{2-}$) [9], thus, the reduction reaction in acidic solution is done very well (in the reactions 7 and 11). Furthermore, electrons in the conduction bond (e_{CB}^-) of the catalyst area can reduce molecular oxygen to a superoxide anion (Eq. (16)) [6].

$$e_{CB}^- + O_2 \rightarrow O_2^{\bullet -} \quad (\mathbf{16})$$

Correspondingly, H_2O_2 is formed by $O_2^{\bullet -}$ in an acidic solution:

$$O_2^{\bullet -} + H^+ \rightarrow HO_2^{\bullet} \quad (\mathbf{17})$$

$$HO_2^{\bullet} + HO_2^{\bullet} \rightarrow H_2O_2 + O_2 \quad (\mathbf{18})$$

$$O_2^{\bullet -} + HO_2^{\bullet} \rightarrow HO_2^- + O_2 \quad (\mathbf{19})$$

$$HO_2^- + H^+ \rightarrow H_2O_2 \quad (\mathbf{20})$$

Therefore, the pair of hydrogen peroxide and oxygen is formed by reactions of 16 to 20 in an acidic solution. According to reaction 11, Cr(VI) is reduced by the hydrogen peroxide.

3.3. The statistical analysis (optimum conditions)

The analysis of variance (ANOVA) consists of a number of statistical methods analyzing the differences between means and their affiliate manners. ANOVA gains the interplay between process variables and responses using a graphical data analysis. To measure the quality of the polynomial model, the researcher used the coefficient of determination (R^2); moreover, its statistical significance was checked by the Fisher's test (F-test). The model condition was evaluated by the probability value (P-value). Table 1 lists the estimated effects and coefficients for x%. This table also reports the values of standard deviation (S), correlation coefficient, pred R-squared and adjusted R-squared. The square of the correlation coefficient for each response was computed as the coefficient of determination (R^2). The accuracy and variability of the model can be evaluated by R^2. The minimum amount of R^2 is 0 and its maximum is 1. The closer the R^2 value to 1, the model is stronger and it predicts the response (x%). The quality of the fittings of the equations was cleared by the coefficient of regression “adjusted R-squared” or in better path by “predicted R-squared”. The “adjusted R-squared” amounts indicate variability in the observed response amounts which can be explained by the experimental variables and their interactions. The “predicted R-squared” and the “adjusted R-squared” values are closer to 1, and a better fitting is attained. The R^2 value was reported to be 0.9996 in this paper. The "pred R-squared" of 0.9743 is in reasonable agreement

with the "adj R-squared" of 0.9988 establishing a better model predictability. Due to Table 1 and the significant variable effects on the response, effects magnitudes on the catalyst amount, pH and concentration of Cr(VI) are respectively equal to 14.80, -13.21 and -11.87. Thus, the considerable reaction parameters were catalyst amount > pH > concentration of Cr(VI). This means that the increase in the primary concentration of the Cr(VI) leads to a decrease in x% and vice versa. In this way, the effects of the variables' interaction were reported in Table 1. In this table, the coefficients of each term have been reported, they are the same term coefficients in the response function and will be obtained by comparing the ratio between the regression mean square and the residual mean square with the appropriate F value. To define the P value, the researcher calculates epsilon statistics based on the sample data and assess the degree that the sphericity hypothesis is broken. Epsilon is multiplied by the numerator and denominator degrees of freedom of the standard test so that a corrected set of degrees of freedom is obtained from the tabled F value, and, thus, its P value is determined.

It is vital to note that P values have been evaluated when α= 0.05. The ANOVA results are shown in Table 2. The response was increased by enhancing the value of F parameter and decreasing P parameter. In this study for every effect, P values are less than 0.05 or equal to zero. In Table 3, supplementary results were gained and were applied in drawing residual plots. The residual values were calculated by subtracting the experimental x% values and fitted values.

A very valuable pictorial presentation of the estimated effects and their statistical importance can be accomplished by using the Pareto chart of the effects. The Pareto chart shows the absolute amounts of the effects on the ordinate. A reference line is drawn in the error margin such that any effect exceeding this reference line is potentially important. The Pareto charts of the effects on the Cr(VI) photocatalytic reduction are shown in Fig. 5.

In order to compare the variables' effect (from the viewpoint of magnitude) on the response, the researcher explores Fig. 5 which is one Pareto chart of the standardized effects. As seen in Fig. 6, the effect of all variables is statistically significant in the process of Cr(VI) photocatalytic reduction. These effects include the decreasing order of the significance and also the amount of photocatalyst, pH and initial concentration of Cr(VI). They are the most important factors affecting the photocatalytic reduction of the Cr(VI); however, they are less important in interactions between variables, (catalyst amount × initial concentration of Cr(VI)) and (pH × initial concentration of Cr(VI)). As can be seen in the Pareto chart, only the catalyst value has a positive effect and the other variables have a negative effect.

Table 1. Estimated effects and coefficients for x%.

Term	Effect	Coef	SE Coef	T (Coef/SE Coef)	P value
Constant		53.17	0.2638	201.55	0.000
Catalyst amount.	29.60	14.80	0.2638	56.10	0.000
pH	-26.42	-13.21	0.2638	-50.08	0.000
Initial Con. of Cr	-23.73	-11.87	0.2638	-44.98	0.000
Catalyst amount × pH	-10.21	-5.10	0.2638	-19.35	0.000
Catalyst amount. × Initial Con. of Cr	-3.73	-1.86	0.2638	-7.06	0.006
pH × Initial Con. of Cr	-3.67	-1.84	0.2638	-6.96	0.006

R^2= 99.96%, pred R^2= 97.43%, adj R^2= 99.88%.

Table 2. ANOVA results.

Source	Degree of freedom	Adj SS	Adj MS	F value
Catalyst amount.	1	1752.62	1752.62	3147.45
pH	1	1396.30	1396.30	2507.55
Initial Con. of Cr	1	1126.46	1126.46	2022.97
Catalyst amount × pH	1	208.39	208.39	374.23
Catalyst amount × Initial Con. of Cr	1	27.79	27.79	49.90
pH × Initial Con. of Cr	1	26.97	26.97	48.44

Table 3. Residual values.

Exp. No.	x%	Fit	Residual (x%–Fit)	St Resid
1	55.10	54.64	0.46	1.71
2	97.73	98.18	-0.45	-1.71
3	41.65	42.10	-0.45	-1.71
4	65.68	65.22	0.46	1.71
5	37.86	38.31	-0.45	-1.71
6	74.85	74.39	0.46	1.71
7	18.88	18.42	0.46	1.71
8	33.64	34.09	-0.45	-1.71
9	51.43	51.46	-0.03	-0.04
10	51.37	51.46	-0.09	-0.14
11	51.58	51.46	0.12	0.19

Fig. 6 illustrates the plots of the three main effects. The variety of the catalyst amounts (ZnO/TD) have only a positive effect on the response (x%). The slope of the line in the main effect plots is one indicator of the magnitude relating to the variable effect on the response. So, the order for affecting variables from magnitude viewpoints is catalyst amount > pH > concentration of Cr(VI). This outcome confirms the results of Fig. 6.

The reduction of the Cr(VI) decreased with increasing the Cr(VI) concentration (As shown in Fig. 6). As the concentrations of potassium dichromate increases, the absorbed light beams in the solution increases as well. For this reason, the light attaining the photocatalyst area is reduced. Therefore, the removal process efficiency decreased [34].

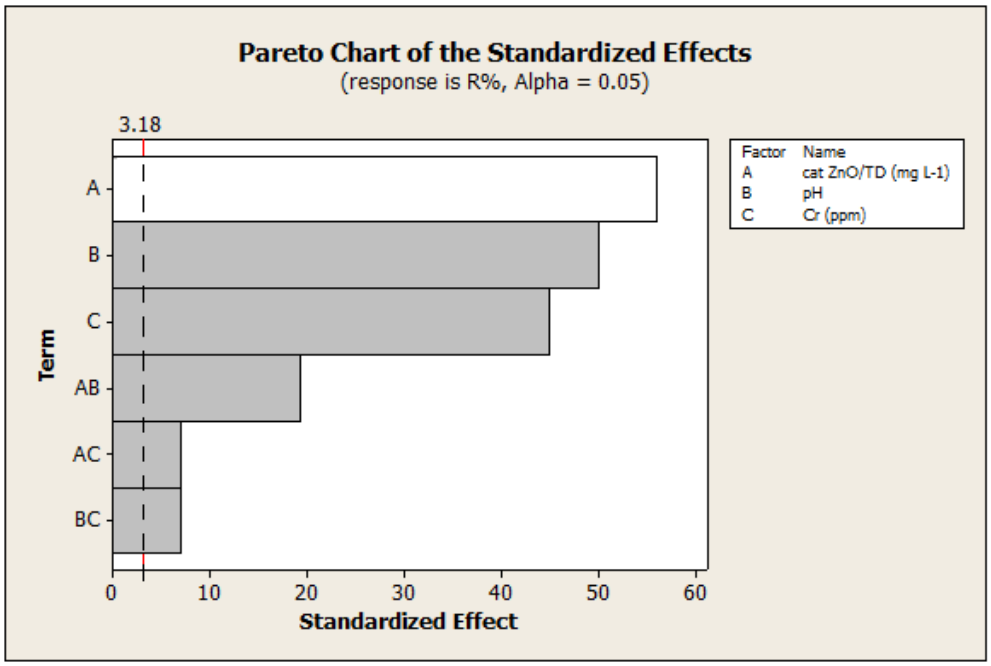

Fig. 5. Pareto chart of the effects on photocatalytic reduction of Cr(VI). White bars: positive effects; gray bars: negative effects. The dotted line is drawn in the error margin.

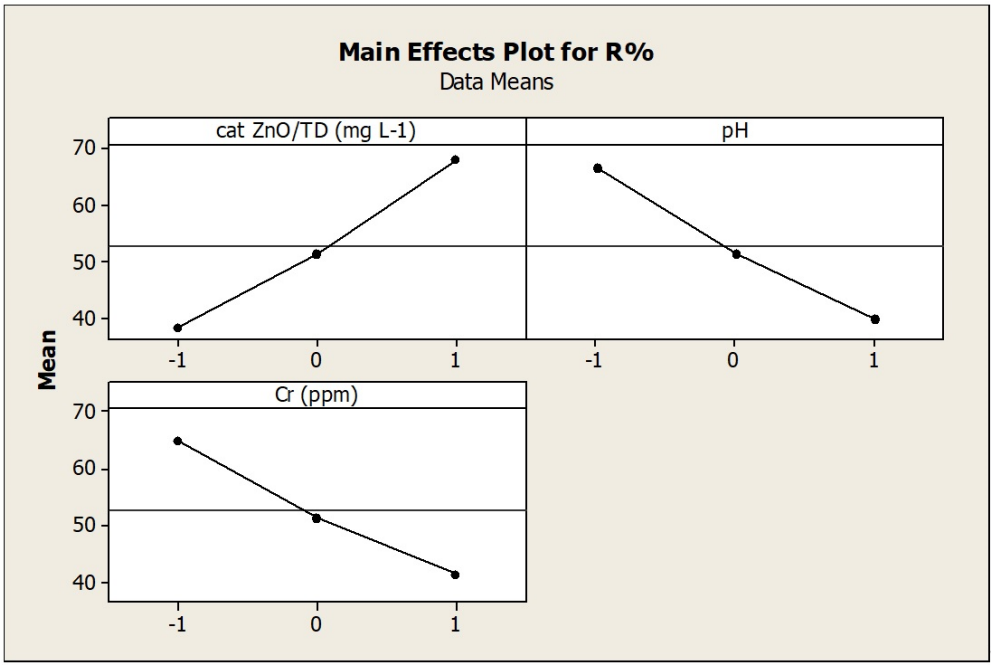

Fig. 6. Main effects plot for x%.

In main effect plots (Fig. 6), those variables whose effects on response is negative (–) or positive (+) have been marked. The results showed that the effect of the amount of catalyst on the x% or other variables but the effect of pH or primary concentration of Cr(VI) variables are negative. For example, the catalyst increase or the pH decrease (or primary concentration of Cr(VI)) leads to an increase of x%. The mathematical model representing Cr(VI) photocatalytic reduction can be presented by the following equation:

Response = x% = 53.17 + 14.80 [ZnO/TD] – 13.21 [pH] – 11.87 [Cr] – 5.10 [ZnO/TD × pH] – 1.86 [ZnO/TD × Cr] – 1.84 [pH × Cr] (**21**)

To determine the reusability of the catalyst, the researcher repeated the experiments 5 times in optimal conditions. Results respectively are as follows: X_1= 98.92, X_2= 98.86, X_3= 98.82, X_4= 98.78, X_5= 98.77. These results show that the reusability of the catalyst is appropriate.

3.4. Kinetics of photocatalytic reduction of Cr(VI)

The plot of ln (A_0/A) versus the reaction time for Cr(VI) photocatalytic reduction was displayed in Fig. 7. The linearity of the plot suggests that the photoreduction reaction approximately follows the pseudo-first order kinetics with a rate coefficient of k= 0.1489 min^{-1}.

The photocatalytic reduction processes following Langmuir-Hinshelwood kinetics are given by Eq. (22):

$$r = -\frac{dC}{dt} = \frac{kKC}{1+KC} \quad (22)$$

Where r is the rate of Cr(VI) photocatalytic reduction, C is the concentration at any time, k is the limiting rate constants of reaction given in the experimental conditions and K is the equilibrium constant for adsorption of Cr(VI) into ZnO/TD particles [35].

The linear relationship is as follow:

$$\left(\frac{1}{r}\right) = \left(\frac{1}{kK}\right) \times \left(\frac{1}{C}\right) + \left(\frac{1}{k}\right) \quad (23)$$

Based on this equation, we can determine the constants of the equation by drawing 1/r in terms of 1/C. The average degradation rate during the first 10 min was calculated as the initial Cr(VI) photocatalytic reduction rate.

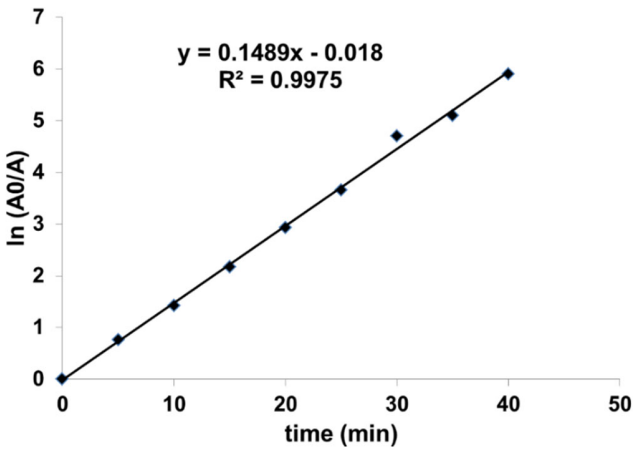

Fig. 7. The plot of the reciprocal of the pseudo-first order rate constant in following conditions: pH= 2, Initial concentration of Cr(VI)= 15 ppm and catalyst amount= 200 mg L^{-1}.

Fig. 8 shows a plot of 1/r versus 1/C in the optimum condition. The values of the k and K were acquired by the linear regression of the points calculated by the reciprocal of L–H model. As a result, k and K were estimated to be 69.93 mmol/min L and 0.0023 L/mmol, respectively.

4. Conclusions

The ZnO NPs is successfully synthesized and supported on the surface of the ZnO/Todorokite. Meanwhile, no chemical change happens to ZnO/Todorokite indicating the effectiveness of this supporting method. The results of XRD show that the supporting of the ZnO has no appreciable effects on the crystal phase of the ZnO and Todorokite. The average crystalline size of the ZnO, NPs support on the TD is 37.83 nm which increases the catalytic activity. After the zinc oxide has stabilized, the energy gap decreased. Supporting ZnO NPs on the area of Todorokite helps to recover them from the medium. The statistical analysis results display that the model used in this paper is significantly reliable and valid.

In the process of the Cr(VI) photocatalytic reduction using ZnO/Todorokite, the three parameters of pH, the initial concentration of Cr(VI) and catalyst amounts have effects on x%. If the interaction effects of the variables are ignored, the variables of the initial concentration of Cr(VI) and pH have a negative effect on the x%. The optimum conditions for the Cr(VI) reduction process by ZnO/Todorokite is when pH= 2, an initial concentration of Cr(VI)= 15 ppm and the catalyst amounts= 200 mg L^{-1} so that they cause to reach a maximum reduction (97.73%). The kinetic of the photocatalytic reduction of Cr(VI) is the pseudo-first order. The process obeys the Langmuir-Hinshelwood kinetics with a good correlation and a linear regression coefficient.

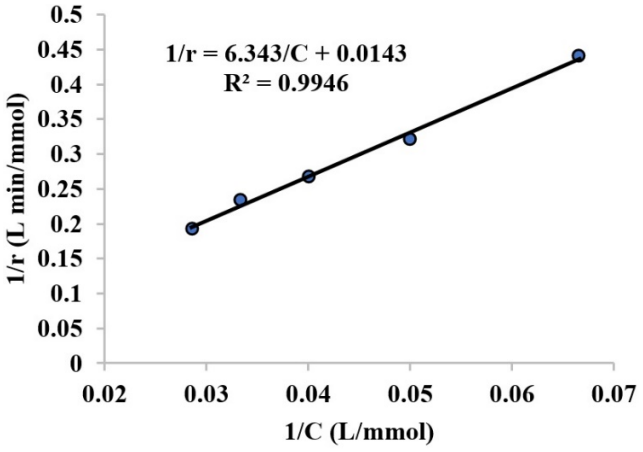

Fig. 8. The plot of 1/r versus 1/C for the experimental data in following conditions: pH= 2, Initial concentration of Cr(VI)= 15 ppm and catalyst amount= 200 mg L^{-1}.

Acknowledgements

The authors are grateful to Islamic Azad University of Arak and the Iranian Nanotechnology Initiative Council.

References

[1] N. Ilankoon, Int. J. Eng. Res. Appl. 4 (2014) 55-63.
[2] Q. Wang, J. Shang, T. Zhu, F. Zhao, J. Mol. Catal. A: Chem. 335 (2011) 242-247.
[3] S. Gupta, B.V. Babu, Bioresour. Technol. 100 (2009) 5633-5640.
[4] M. Kebir, M. Chabani, N. Nasrallah, M. Trari, Desalination 270 (2011) 166-173.
[5] G. Colón, M.C. Hidalgo, J.A. Navío, J. Photochem. Photobiol. A 138 (2001) 79-85.
[6] A. Nezamzadeh-Ejhieh, Z. Banan, Desalination 279 (2011) 146-151.
[7] H.R. Pouretedal, M. Fallahgar, F. Sotoudeh Pourhasan, M. Nasiri, Iran. J. Catal. 7 (2017) 317-326.
[8] L. Vafayi, S. Gharibe, Iran. J. Catal. 5 (2015) 365-371.
[9] A. Nezamzadeh-Ejhieh, G. Raja, J. Chem. 2013 (2013) 1-13.
[10] S. Wang, Z. Wang, Q. Zhuang, Appl. Catal. B 1 (1992) 257-270.
[11] Ü. Özgür, Ya.I. Alivov, C. Liu, A. Teke, M.A. Reshchikov, S. Doğan, V. Avrutin, S.-J. Cho, H. Morkoç, J. Appl. Phys. 98 (2005) 041301.
[12] B. Khodadadi, M. Bordbar, Iran. J. Catal. 6 (2016) 37-42.
[13] M. Giahi, A. Hoseinpour Dargahi, Iran. J. Catal. 6 (2016) 381-387.
[14] N. Manavizadeh, A.R. Khodayari, A. Asl Soleimani, S. Bagherzadeh, Iran. J. Chem. Chem. Eng. 31 (2012) 37-42.
[15] G. Al-Dahash, W. Mubdir Khilkala, S.N. Abdul Vahid, Iran. J. Chem. Chem. Eng. 37 (2018) 11-16.
[16] F.A. Al-Sagheer, M.I. Zaki, Microprous Mesporous Mater. 67 (2004) 43-52.
[17] R. Nabizadeh, M. Jahangiri Rad, Res. J. Nanosci. Nanotechnol. 6 (2016) 1-7.
[18] V.A. Sakkas, M.A. Islam, C. Stalikas, T.A. Albanis, J. Hazard. Mater. 175 (2010) 33-44.
[19] J. Fernández, J. Kiwi, C. Lizama, J. Freer, J. Baeza, H.D. Mansilla, J. Photochem. Photobiol. A. Chem. 151 (2002) 213-219.
[20] M.C. Yeber, C. Soto, R. Riveros, J. Navarrete, G. Vidal, Chem. Eng. J. 152 (2009) 14-19.
[21] M. Sabonian, M.A. Behnajady, Desalin. Water Treat. 56 (2014) 1-11.
[22] S.V. Balakhonov, B.R. Churagulov, E.A. Gudilin, J. Surf. Invest. 2 (2008) 152-155.
[23] A. Chen, S. Xia, X. Pan, H. Lu, Z. Ji, J. Alloys. Compd. 735 (2018) 1314-1318.
[24] Z. Ren, X. Liu, H. Chu, H. Yu, Y. Xu, W. Zheng, W. Lei, P. Chen, J. Li, C. Li, J. Colloid Interface Sci. 488 (2017) 190–195.

[25] F. Jing, R. Liang, J. Xiong, R. Chen, S. Zhang, Y. Li, L. Wu, Appl. Catal. B 206 (2017) 9–15.
[26] G. Corro, N. Sánchez, U. Pal, S. Cebada, J.L. García Fierro, Appl. Catal. B 203 (2017) 43–52.
[27] Y. Z, C. Luo, L. Liu, Z. Yang, S. Ren, Y. Cai, J. Xiong, Mater. Lett. 181 (2016) 169–172.
[28] M. Hamadanian, A. Sadeghi Sarabi, A. Mohammadi Mehra, V. Jabbari, Mater. Sci. Semicond. Process. 21 (2014) 161–166.
[29] X. Han Feng, M. Zhu, M. Ginder-Vogel, C. Ni, S.J. Parikh, D.L. Sparks, Geochim. Cosmochim. Acta. 74 (2010) 3232–3245.
[30] M. Bordbar, S. Forghani-pilerood, A. Yeganeh-Faal, Iran. J. Catal. 6 (2016) 415-421.
[31] S. Aghdasi, M. Shokri, Iran. J. Catal. 6 (2016) 481-487.
[32] Z. Jin, Y.X. Zhang, F.L. Meng, Y. Jia, T. Luo, X.Y. Yu, J. Wang, J.H. Liu, X.J. Huang, J. Hazard. Mater. 276 (2014) 400-407.
[33] K. Kabra, R. Chaudhary, R.L. Sawhney, Ind. Eng. Chem. Res. 43 (2004) 7683-7696.
[34] S. Chakrabarti, B. Chaudhuri, S. Bhattacharjee, A.K. Ray, B.K. Dutta, Chem. Eng. J. 153 (2009) 86-93.
[35] A. Nezamzadeh-Ejhieh, Z. Ghanbari-Mobarakeh, J. Ind. Eng. Chem. 21 (2015) 668-676.